Review Article

Charge breeding time investigations of electron cyclotron resonance charge breeders

Julien Angot,[1,*] Olli Tarvainen,[2] Thomas Thuillier,[1] Maud Baylac,[1] Thierry Lamy,[1] Patrick Sole,[1] and Josua Jacob[1]

[1]*Université Grenoble Alpes, CNRS, Grenoble INP, LPSC-IN2P3, 38000 Grenoble, France*
[2]*University of Jyvaskÿlä, Departement of Physics, 40500 Jyväskylä, Finland*

(Received 19 July 2018; published 30 October 2018)

To qualify electron cyclotron resonance charge breeders, the method that is traditionally used to evaluate the charge breeding time consists in generating a rising edge of the injected beam current and measuring the time in which the extracted multicharged ion beam reaches 90% of its final current. It is demonstrated in the present paper that charge breeding times can be more accurately measured by injecting short pulses of 1 + ions and recording the time resolved responses of N+ ions. This method is used to probe the effect of the 1 + ion accumulation in the plasma known to disturb the buffer gas plasma equilibrium and is a step further in understanding the large discrepancies reported in charge breeding times. The experiments are conducted injecting a $^{85}Rb^{+}$ ion beam into the Laboratoire de Physique Subatomique et de Cosmologie (LPSC) charge breeder operated with helium as a buffer gas. The time needed for the extraction of 90% of the multicharged ions in short pulse mode is found slightly shorter (9%) than the charge breeding time measured with the traditional method. The charge breeding efficiency is identical with both methods. The pulse width and amplitude of the 1+ injection pulses have been varied to study their influence on the N+ response and temporal parameters are proposed to qualify the time response. The short pulse method can be used to study the influence of the ion source tuning parameters on the charge breeding temporal characteristics. For example, it is shown here that an increase of the minimum magnetic field strength of the LPSC charge breeder in the range 0.432–0.444 T improves the multicharged ion confinement in the electron cyclotron resonance plasma, and so increases the charge breeding efficiency. The short pulse method is also used to estimate the charge breeding efficiencies of radioactive Rb isotopes taking into account their half-lives and charge states. The neutron-rich heavy isotopes have short half-lives, which makes the charge state distributions shift to lower charge states and the estimated charge breeding efficiencies of high charge states being close to three times less in comparison to the stable ions.

DOI: 10.1103/PhysRevAccelBeams.21.104801

I. INTRODUCTION

Electron cyclotron resonance ion sources (ECRIS) are used as charge breeders (CB) in radioactive ion beam (RIB) facilities using the "isotope separation on line" (ISOL) scheme [1]. The radioactive atoms are produced through nuclear fission induced by the interaction between a primary beam and the target material. After being ionized to form a 1+ beam in a target ion source at the yield in the range of 10^4–10^{11} particles per second, the radioactive species are separated in a mass spectrometer. The charge breeder increases the RIB charge state from 1+ to N+, favoring an efficient postacceleration of RIBs to high energy. The performance of the charge breeder is characterized by the following parameters:

First, the charge breeding time τ_{CB} represents the characteristic time required for the injected ions to be charge bred to the desired charge state. This parameter is a key point to avoid decay losses of the radioactive ions during the charge breeding. Ions having a short half-life (on the order of 1 s or less) are expected for physics experiments, for example at the SPIRAL1 upgrade [2] or CARIBU [3]. τ_{CB} is typically expressed either directly in milliseconds or in units of milliseconds per charge state (ms/q), which highlights the stepwise nature of the ionization process but at the same time suggests the fact that the charge breeding time increases linearly with the charge state. This assumption is only true for highly charged ions [2] but is used for all the charge state distribution as an approximation. It allows one to estimate if the desired charge state is reachable as a function of the RIB half-life.

Second, the efficiency for a single charge state is defined as the ratio between the extracted particle current at the

*Corresponding author.
Julien.angot@lpsc.in2p3.fr

given charge state and the injected particle current. Since the RIB production yield may be very low, down to 10^4 particles per second or even lower, the charge breeding efficiency is also a crucial point.

The third parameter is the CB beam purity defined as the percentage of chemical contaminant elements included into the N+ beam of interest. The contaminants having the same m/q value with the RIB can be detrimental or even prohibitive for the physics experiments conducted with the postaccelerated ions especially in the case of low production yield.

The ECR charge breeding technique is based on the use of a modified minimum-B ECR ion source. A port is added on axis to allow the injection of the low charge state ion beam. The incoming beam is first electrostatically decelerated (see Sec. II for details), then by the plasma potential, and finally by Coulomb collisions with the plasma ions. An optimum of the capture is reached when the speed of the injected ions is equal to the average speed of the plasma ions [4]. When trapped by the magnetized plasma, the injected ions behave like other plasma ions: they are multiionized and extracted along with the buffer gas ions like in conventional ECR ion sources.

The charge breeding time τ_{CB} is traditionally experimentally quantified with the process which consists in generating a rising edge of the injected beam (1+) with an electrostatic steerer and measuring the rise time of the charge bred (N+) signal [5–8]. To obtain a better signal-to-noise ratio, the response is usually averaged over several measurements, requiring a pulsing of the injected beam. The pulse signal frequency has to be adjusted in order to allow enough time for the N+ signal to reach its saturation value, for both the rising and falling edges. The rise and fall response times are typically in the same order of magnitude, and thus the pulsing signal is often generated with a duty cycle of approximately 50%. Figure 1 illustrates this principle with $^{85}Rb^{20+}$. In the given example the charge breeding time is 330 ms (16.5 ms/q).

In the case of the ISOL method where the ions of interest are very difficult and expensive to produce, a fraction of 90% is considered to be a suitable value for the radionuclide conservation through the charge breeder. In other words, the 90% breeding time should be less than the characteristic decay time of the radioactive species. Therefore the timing is triggered by the command signal and the time when the extracted N+ beam current reaches 90% of its final value is considered as the charge breeding time.

The evolution of the N+ intensity shown in Fig. 1 is driven by the accumulation of the injected ions in the CB plasma and the relaxation of the CB plasma into a new equilibrium, which can be affected by the accumulation of the injected species. Strong perturbation of the plasma can be induced, sometimes triggering an unstable mode of operation, depending on the 1+ beam and the charge breeder plasma characteristics. For example, with the LPSC

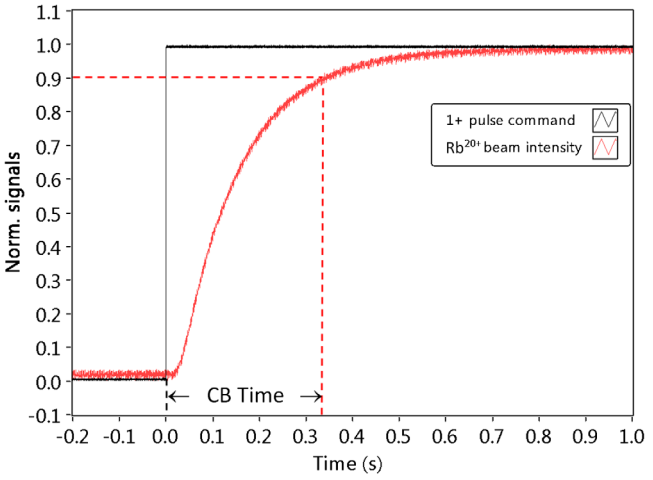

FIG. 1. Principle of the traditional τ_{CB} measurement. Dashed lines are the references of the pulse start (black) and 90% level of the Rb^{20+} beam intensity (red).

charge breeder, a 50% decrease of the O^{6+} beam current has been induced by a continuous injection of 1 μA of Cs^+ ions [9]. Experiments have also demonstrated that, for particular magnetic configurations, the accumulation of injected Cs in the plasma can trigger kinetic instabilities which cause the charge breeding efficiency to collapse [10].

In Fig. 1, 400 ms after the injection starts, the N+ signal is still increasing but the moment of the injection of the 1 + ions contributing to the extracted N+ current at this stage is questionable; some ions may have been injected at the beginning of the 1+ pulse while some of them have been injected later. Thus, the actual τ_{CB} is defined ambiguously, which makes it difficult to compare charge breeding times measured with different charge breeders and operational parameters.

Table I summarizes reported performances from the SPIRAL1 (GANIL, France) [2], CARIBU (ANL, USA) [3,11], and LPSC (France) [12] charge breeders. Large variations can be seen especially in the reported τ_{CB}. For ^{39}K, τ_{CB} ranges between 3.9 and 16.7 ms/q with a noticeable increase of the efficiency with the reported τ_{CB}, which implies that the charge breeding has a direct connection to the ion confinement properties of ECRIS plasmas. A substantial decrease of τ_{CB} was observed with the SPIRAL1 charge breeder for $^{39}K^{9+}$ by changing the support gas from He (13 ms/q) to H_2 (3.9 ms/q), without a major modification of the CB tuning parameters. In this case, the efficiency decreased only slightly from 13.0% to 11.7%.

Other charge breeder parameters such as the magnetic field strength, the microwave power, and the microwave frequency have also been found to act on τ_{CB} [3]. For example, at Argonne National Laboratory, for $^{132}Xe^{26+}$, a substantial increase from 8.8 to 46.1 ms/q was measured after slightly changing the microwave frequency from 11.762 to 11.765 GHz. At LPSC, a value of 5.9 ms/q was measured for this charge state and element during recent experiments.

TABLE I. Examples of efficiencies and τ_{CB} of K and Xe, measured at the conditions corresponding to the best achieved efficiencies or the best compromise between τ_{CB} and efficiency, with the SPIRAL1, CARIBU, and LPSC charge breeders.

		SPIRAL1		CARIBU		LPSC	
Ion	A/q	Efficiency (%)	τ_{CB} (ms/q)	Efficiency (%)	τ_{CB} (ms/q)	Efficiency (%)	τ_{CB} (ms/q)
$^{39}K^{10+}$	3.9			17.9	15.7	11.7	8.2
$^{39}K^{9+}$	4.33	13.0	13.0	15.6	16.7		
$^{39}K^{9+}$	4.33	11.7	3.9				
$^{132}Xe^{26+}$	5.07			13.5	46.1	13.3	5.9
$^{132}Xe^{26+}$	5.1			10	8.8		

The accumulation effect and the large discrepancies of the reported τ_{CB} have motivated the authors to conduct charge breeding experiments in short pulse mode, as early proposed in [13]. Short 1+ pulses, in the order of 1 ms long, were injected into the CB buffer gas plasma at equilibrium, and N+ responses were studied. In this configuration, all the extracted ions are injected during a time interval which is significantly shorter than τ_{CB} and the N+ response is then mainly driven by the ionization and confinement times, not by the accumulation of injected ions and a possible gradual change of the plasma parameters towards a new equilibrium. It is shown in the following sections, using Rb as an example, that such a method allows one to measure the charge breeding time accurately and makes it possible to predict breeding efficiencies of radioactive ions based on experiments with stable isotopes.

Earlier experiments with short pulse material injection into minimum-B ECRIS plasmas have been aiming to estimate the values of certain plasma parameters. The injection of neutral particles was achieved, by means of laser ablation, target sputtering, and fast gas injection [14–16]. The superposition of the N+ beam responses has clearly illustrated the step-by-step ionization process. The intensities and time constants of the signals were used to calculate the plasma electron density n_e, the plasma electron temperature T_e, and the confinement time τ_c, like initially proposed in [17]. The effect of several source parameters such as the bias disc potential, microwave power, buffer gas pressure, and magnetic confinement have been studied with several species including bismuth, gold, aluminum, cadmium, and argon. Although such experiments are valuable for determining the plasma parameters (under certain assumptions), their results cannot be translated directly to predicting the charge breeding times of 1+ injected ions in CB-ECRISs.

II. EXPERIMENTAL SETUP

All of the experimental data presented hereafter was taken with the PHOENIX charge breeder, a 14.5 GHz minimum-B ECR ion source developed at LPSC since 2000 [18], on the 1+ → N+ test bench (Fig. 2).

The 1+ beam line section is dedicated to the production of the injected beam. Two types of low charge state ion sources (1 + ion sources) are used: a COMIC source [19]

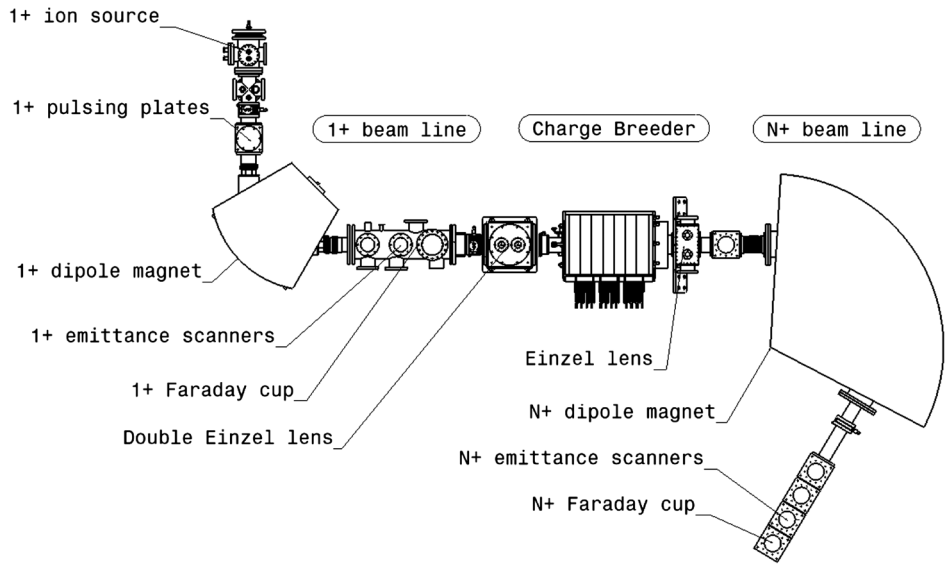

FIG. 2. Schematic layout of the 1+ → N+ test bench.

for gaseous elements and an ion gun [20] for alkalis, the latter one being used in this work. After extraction, the beam passes through the 1+ pulsing system composed of two horizontal plates that is used in long pulse mode for the traditional τ_{CB} measurement method. One plate is grounded and the other one is connected to a switching system based on the use of a field effect transistor that connects a 250 V deflection voltage to the plate. The switching system is driven by the command and control program that generates a square signal via the data acquisition board of the computer. Downstream, the beam line is composed of a 90° dipole magnet for the 1+ beam selection and a diagnostic chamber equipped with two Allison type emittance scanners, one Faraday cup, and two magnetic steerers. Finally, a double Einzel lens is set to optically adapt the beam to the charge breeder entrance.

The charge breeder was configured as follows. At injection, a large diameter electrode is set in the insulator to ensure a correct 1+ beam guiding during the 1+ beam deceleration [21]. In the plasma chamber an "high frequencies blocker" electrode [21] reduces the leak of microwaves towards the injection. The two soft iron rings surrounding the hexapole are set at their maximum position at the extraction side. In this configuration, the maximum magnetic field strengths achievable are 1.2 T at injection and 0.9 T at extraction. The magnetic field of the charge breeder is thoroughly described in [20].

The N+ beam line section is devoted to the analysis of the beam extracted from the charge breeder. First an Einzel lens is placed at the charge breeder extraction to adapt the beam to the 120° dipole magnet. Finally, two Allison type emittance scanners and a Faraday cup are installed in the last section to diagnose the A/Q-analyzed N+ beams.

The 1+ source potential, usually 20 kV, is set by a high-voltage supply and the charge breeder is biased relative to the 1+ source by a negative voltage supply referred to as ΔV. In this configuration, the energy of the decelerated 1+ beam entering the charge breeder can be fine-tuned allowing the optimization of the final speed of the ions, and so the trapping efficiency. The ΔV power supply together with the 1+ source electronics, are set on a high-voltage platform and the charge breeder electronics on another one.

The pulsing plates were reused to implement the short pulse method described in the first paragraph. However, as the pulse duration had to be tuned and carefully defined to manage the amount of injected particles, the command signal was delivered by a more accurate signal generator. The rise and fall times of the voltage applied to the pulsing plate were respectively measured at 2 and 60 μs, while the rise time of the beam in the 1+ Faraday cup was measured to be shorter than 40 μs.

The pulse signal was generated with the following constraints: (i) The pulse duration has to be short with respect to the N+ beam response. (ii) The number of injected particles has to be high enough to allow a good signal-to-noise ratio of the N+ signal. (iii) The 1+ pulse frequency has to be sufficiently low to allow the extraction of all the injected ions and a possible relaxation of the CB plasma before the injection of the following pulse.

III. EXPERIMENTAL RESULTS

A. Pulse response

The short pulse method for the charge breeding time measurement was tested injecting an $^{85}Rb^{+}$ beam into the charge breeder operating with He as buffer gas. The microwave power level was 510 W. The injection, minimum, and extraction axial magnetic field strength were simulated to be 1.19, 0.44, and 0.84 T, respectively (injection, median, and extraction coils were set at 1185, 320, and 726 A). An efficiency of 4.8% was achieved for Rb^{19+} with an injected beam intensity of 791 nA. The 1+ beam was then pulsed at 0.4 Hz, and the Rb^{19+} signal was recorded with an oscilloscope from the N+ Faraday cup. The pulse duration was decreased until the temporal behavior of the normalized N+ response was not affected anymore. Figure 3 shows the response of the Rb^{19+} current to a 2.5 ms 1+ injection pulse (about 1.2×10^{10} particles injected), together with the integral of this signal, i.e., the cumulative distribution function. In this figure, like in all the following ones, the origin of the horizontal axis is set at the beginning of the 1+ pulse command.

In pulse mode, the efficiency was measured similar to the traditional mode, i.e., by calculating the ratio of N+ particles outgoing ions on 1+ incoming ones as $\eta_{N^+} = \frac{\int I_{N^+} dt}{N \int I_{1^+} dt}$ where I_{1^+} and I_{N^+} are, respectively, the 1+ and N+ pulse intensities and N the ion charge state number. This method gave an efficiency of 4.8% for Rb^{19+}, identical to the value obtained with the traditional method

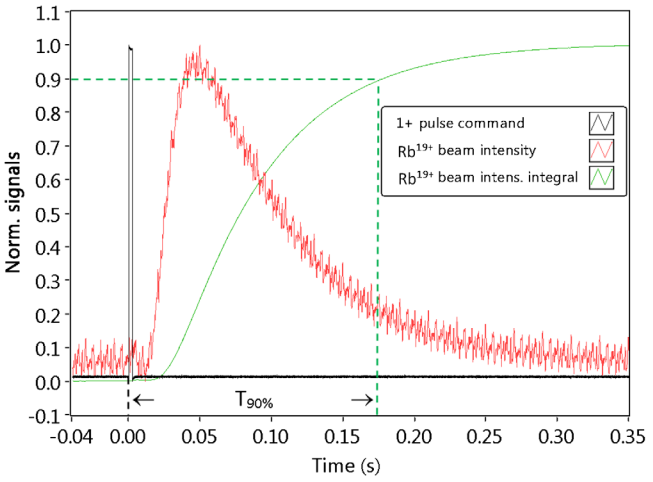

FIG. 3. Rb^{19+} response to a 2.5 ms injected pulse and the corresponding integral function. Dashed lines are the references of the pulse start (black) and 90% level of the Rb^{19+} integral function (green).

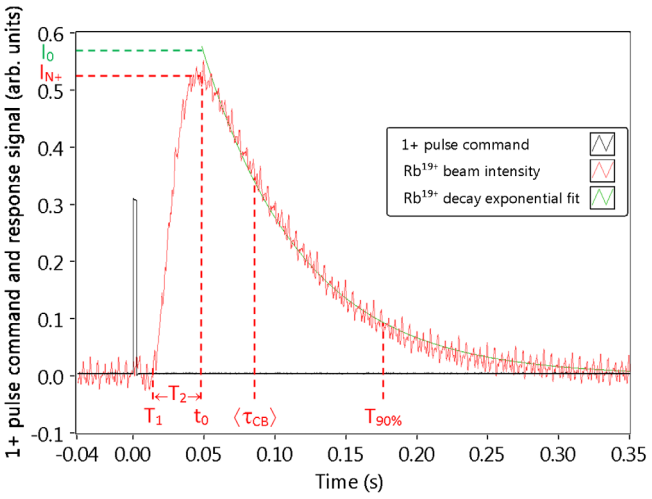

FIG. 4. Red: Rb^{19+} response to a 2.5 ms injected pulse and characteristic parameters (see text for details). Black: 1+ injection pulse. Green: Exponential fit of the pulse decay.

applied with continuous injection of the $1+$ ions. The comparison of the efficiencies demonstrates that the charge breeding process is probed at the same plasma conditions or breeding efficiencies with both, the short-pulse and traditional methods.

For the same reasons as in the traditional method, we consider here a value of 90% for the proportion of the extracted ions to define the charge breeding time, which allows comparing τ_{CB} with both the traditional and short-pulse methods. The corresponding time $T_{90\%}$ is defined between the start of the injected 1+ pulse and the time when 90% of the N+ ions have been extracted. In the case of Fig. 3, $T_{90\%}$ was measured to be 178 ms. Using the traditional method, τ_{CB} was measured to be 191 ms. The pulsed method gives a charge breeding time shorter by 9%, the difference being most likely due to the accumulation effect (i.e., self-consistent perturbation of the buffer plasma due to $1+$ ion accumulation).

B. Studies of the accumulation effect

To study the accumulation effect, several characteristic parameters were defined from the N+ response curve as shown in Fig. 4: T_1 is the time between the start of the 1+ injection pulse and the first appearance of the N+ ions of the given charge state in the extracted beam. It is the necessary time for ionization cascade of the lower charge states to reach the value N. T_2 is the signal rise time from the first appearance of N+ ions to its maximum I_{N+}. This parameter illustrates the speed at which the N+ ions are produced by ionization from the $N-1$ charge state and by charge exchange and recombination from the $N+1$ charge state, the ionization dominating in this case [22]. The decay of the N+ response is fitted with an exponential curve $i(t) = I_0 e^{\frac{-t+t_0}{\tau}}$, where τ is a measure of the characteristic decay time and $t_0 = T_1 + T_2$. The fit is done with the least square method. It can be argued that τ depicts the characteristic time of the N+ ion confinement in the ECR plasma.

In addition, the N+ response signal can be considered as a temporal probability distribution function of N^+ ion emission from the plasma.

The temporal average of the distribution function is $\tau^{N+} = \langle t \rangle = \frac{\int_0^\infty t I^{N+}(t)dt}{\int_0^\infty I^{N+}(t)dt}$ where time 0 is taken at the 1+ rise time.

The average CB time is the difference between the temporal average of the N+ response and the temporal average of the 1^+ pulse signal: $\langle \tau_{CB} \rangle = \tau^{N+} - \tau^{1+}$. The standard deviation is $\sigma_\tau^{N+} = \sqrt{\langle t^2 \rangle - \langle t \rangle^2}$.

In the case of Fig. 4 the characteristics parameters were measured as $T_1 = 13.0$ ms, $T_2 = 33.7$ ms, $I_{N+} = 18.4$ nA, $\tau_{CB} = 92.5$ ms, $\sigma_\tau^{N+} = 60.4$ ms, $T_{90\%} = 177.5$ ms, $I_0 = 20.5$ nA, and $\tau = 70.8$ ms.

Table II summarizes the fractions of extracted particles at various $\langle \tau_{CB} \rangle$ and σ.

In this case, the average statistical charge breeding time $\langle \tau_{CB} \rangle$ is about two times shorter than $T_{90\%}$. Altogether, the statistical parameters and $T_{90\%}$ allow one to qualify the N+ response as follows.

1. *Effect of the* 1+ *pulse width*

The effect of the 1+ pulse duration on the parameters listed above was studied in the same CB configuration. Figure 5 shows representative Rb^{19+} pulse responses for 0.625, 2.5, 10, 40, and 160 ms 1+ pulse durations.

Figure 5(a) shows that when the 1+ pulse duration is less than 10 ms, i.e., less than T_1, it has practically no influence on the normalized Rb^{19+} response. This is clearly visible by plotting the evolution of the characteristic times as a function of the pulse duration [Fig. 5(b)]. Beyond 10 ms, the rise time T_2 starts to increase, following the pulse duration slope for pulse durations >80 ms. T_1 is unaffected, which can be expected as it reflects the time required for the ionization cascade to reach the given charge state. $T_{90\%}$, that can be compared to the traditional CB time T_{tradi}, starts to increase while $\langle \tau_{CB} \rangle$ and τ decrease when the pulse length exceeds 20 ms. Beyond this value, the accumulation effect increasingly changes the plasma and its characteristic values like the confinement time and $\langle \tau_{CB} \rangle$. In conclusion, we can say that to avoid the accumulation effect when measuring the charge

TABLE II. Fraction of extracted particles as a function of $\langle \tau_{CB} \rangle$ and σ.

Time	$\langle \tau_{CB} \rangle - \sigma$	$\langle \tau_{CB} \rangle$	$\langle \tau_{CB} \rangle + \sigma$	$\langle \tau_{CB} \rangle + 2\sigma$	$\langle \tau_{CB} \rangle + 3\sigma$
Proportion of extracted particles (%)	9.7	61.0	85.2	94.8	98.4

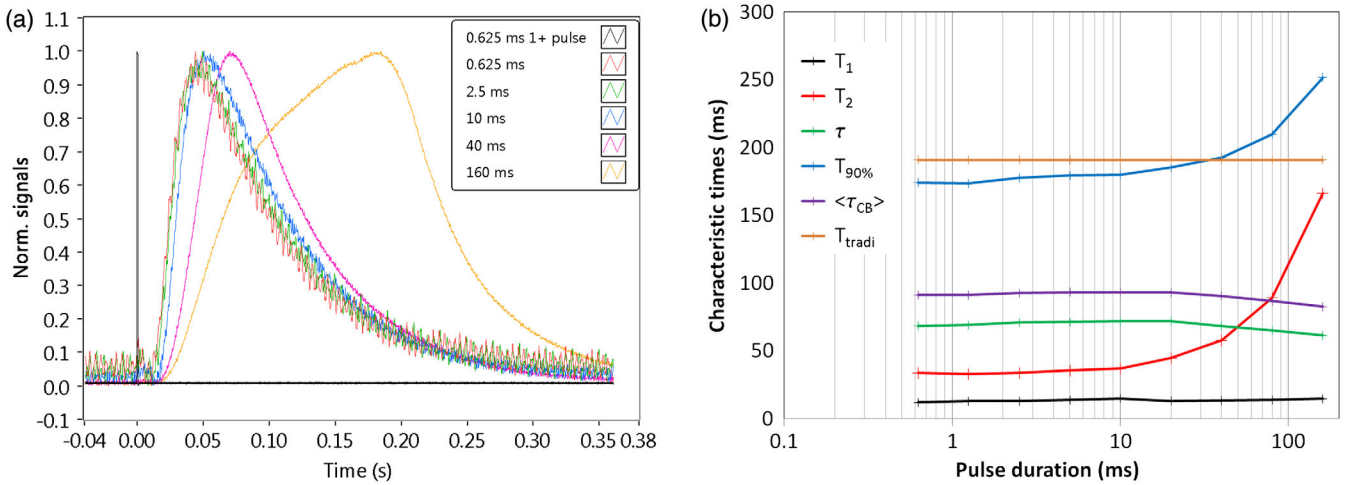

FIG. 5. (a) 0.625 ms pulse command and normalized Rb^{19+} response to 0.625, 2.5, 10, 40, and 160 ms 1+ pulses. (b) Characteristic times as a function of the 1+ pulse duration. Characteristic time parameters uncertainty is evaluated at ±3%.

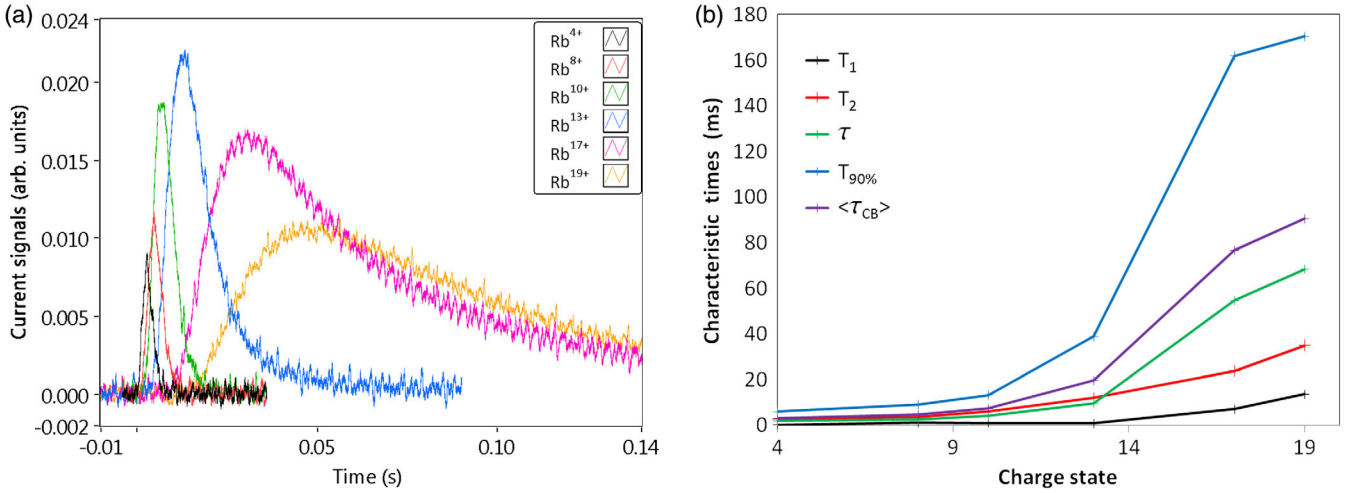

FIG. 6. (a) Rb^{4+}, Rb^{8+}, Rb^{10+} Rb^{13+}, Rb^{17+}, and Rb^{19+} beam intensities responses to a 2.5 ms pulse. (b) Evolution of the characteristic times as a function of the Rb charge state. The characteristic time parameters uncertainty is evaluated at ±3%.

breeding time, the 1+ pulse duration has to be shorter than T_1.

2. Rb charge state

The responses of Rb^{4+}, Rb^{8+}, Rb^{10+}, Rb^{13+}, Rb^{17+}, and Rb^{19+} currents to 2.5 ms 1+ injection pulses were measured and are compared in Fig. 6(a). The order of appearance (and disappearance) of the pulses reflects the nature of the stepwise ionization process and time evolution of the charge state distribution.

The evolution of the time characteristics as a function of the ion charge state is illustrated in Fig. 6(b) and the parameters are summarized in Table III. The ratio of $T_{90\%}$ and $\langle\tau_{CB}\rangle$ is constant for all of the charge states. A clear

TABLE III. Characteristic N+ pulse temporal parameters as a function of Rb ion charge state.

Charge state	T_1 (ms)	T_2 (ms)	τ (ms)	$T_{90\%}$ (ms)	$\langle\tau_{CB}\rangle$ (ms)	σ (ms)	Pulse Efficiency (%)
4	0.1	2.7	1.8	6.0	2.9	4.7	0.7
8	1	3.6	2.6	8.9	4.7	3.8	0.6
10	0.9	5.9	4.0	13.1	7.3	4.3	1.3
13	0.9	12.0	9.6	38.8	19.6	15.0	2.6
17	7	23.8	54.6	161.8	76.6	61.4	6.4
19	13.6	34.9	68.3	170.3	90.4	55.5	5.1

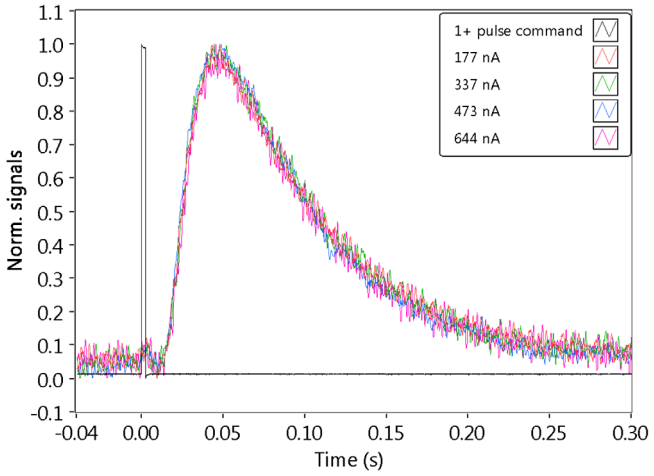

FIG. 7. 1+ injection pulse and Rb^{19+} normalized signal responses to several 1+ beam pulse intensities.

correlation among $T_{90\%}$, τ, and $\langle\tau_{CB}\rangle$ can be seen for high charge states ≥13. The maximum pulse duration avoiding accumulation effect depends on T_1 and hence, the ion charge state.

3. *Effect of the* 1+ *pulse intensity*

The influence of the 1+ beam intensity on the characteristic times was studied by injecting pulses of 177, 337, 473, and 644 nA lasting 2.5 ms (Fig. 7).The charge breeder was set in the same configuration as before. Figure 7 shows a perfect similarity of the Rb^{19+} responses when normalized with respect to the maximum current, which implies that the plasma perturbation caused by the short pulse is negligible at these currents. Further experiments at higher beam intensities would be necessary to find the limit where the 1+ beam injection and ion accumulation into the plasma would perturb it enough to skew the temporal response.

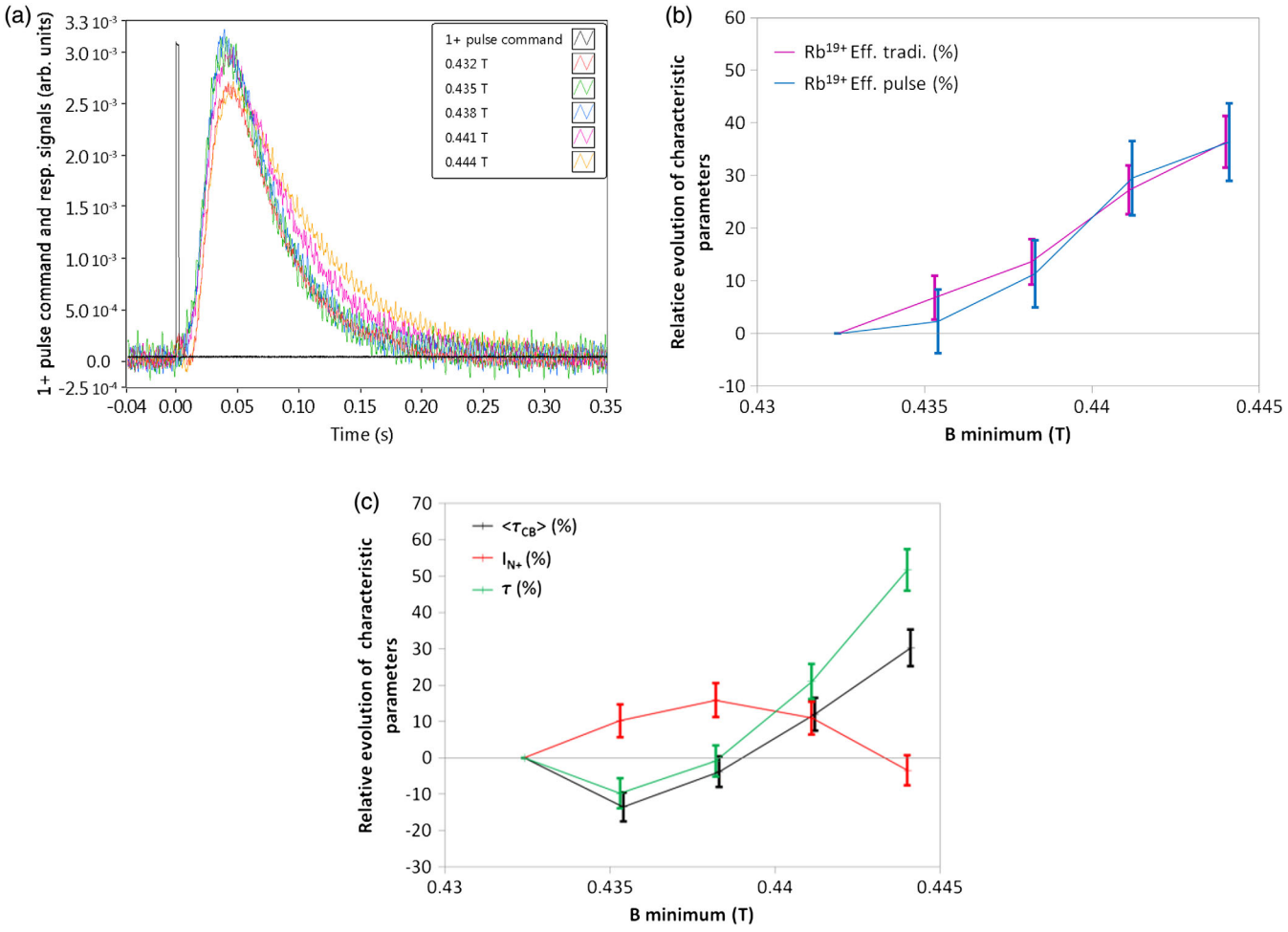

FIG. 8. (a) Rb^{19+} signal responses at several median coil currents. (b) Variation of the Rb^{19+} efficiency as a function of the median axial field. (c) Variation of the time characteristics and maximum current as a function of the median axial field. (b), (c) Relative uncertainty on the estimated B minimum field plotted on the x axis is evaluated at ±0.5%.

4. Magnetic field effect

In this study, we pay attention to the influence of the median axial magnetic field (B-minimum) of the charge breeder on the rubidium charge breeding process. The median coil current was varied from 300 to 320 A with 5 A steps leading to a variation of the magnetic field from 0.432 to 0.444 T, all other parameters being left unchanged. A Rb^{+} beam was injected either in long pulses (2000 ms/177 nA), or in short pulses (2.5 ms/177 nA). The Rb^{19+} production efficiency was calculated for both injection schemes; the Rb^{19+} temporal evolution was recorded when injecting short pulses. Figure 8(a) shows the temporal evolution of the Rb^{19+} signal for each magnetic field value; Fig. 8(b) shows the variation of some charge breeding parameters with respect to their value at 0.432 T (Rb^{19+} efficiency in both injection schemes, peak intensity of the Rb^{19+} signal, characteristic decay time, $\langle \tau_{CB} \rangle$).

Concerning the efficiency, the magnetic field increase resulted in a continuous increase of the Rb^{19+} efficiency from 4.4% to 6.0% and the values do not differ between the two injection schemes; see Fig. 8(b). In the given range, the peak intensity I_{N+} has a maximum at 0.438 T, while the characteristic decay time τ first decreases before increasing significantly as the B-minimum becomes higher [Fig. 8(c)]. Since the decay time can be considered to be directly related to the confinement time of the high charge state ions [23], the result implies that at stronger B-minimum the ion confinement is improved. The Rb^{19+} efficiency increase in the range seems to be linked to both I_{N+} and τ parameters, which is consistent with the presumably improved confinement of high charge state ions.

With a median axial magnetic of 0.435 T, the efficiency is 22% lower than at 0.444 T but at the same time the average τ_{CB} is 34% shorter at lower field. This illustrates the compromise between τ_{CB} and the efficiency that may be necessary in case of a short half-life isotope.

This study shows how the short pulse beam injection can be used to compare the charge breeder tuning parameters like the support gas and the plasma heating frequency. It is a new tool that will help us to understand the large variations of the reported efficiencies and CB times measured with the traditional method.

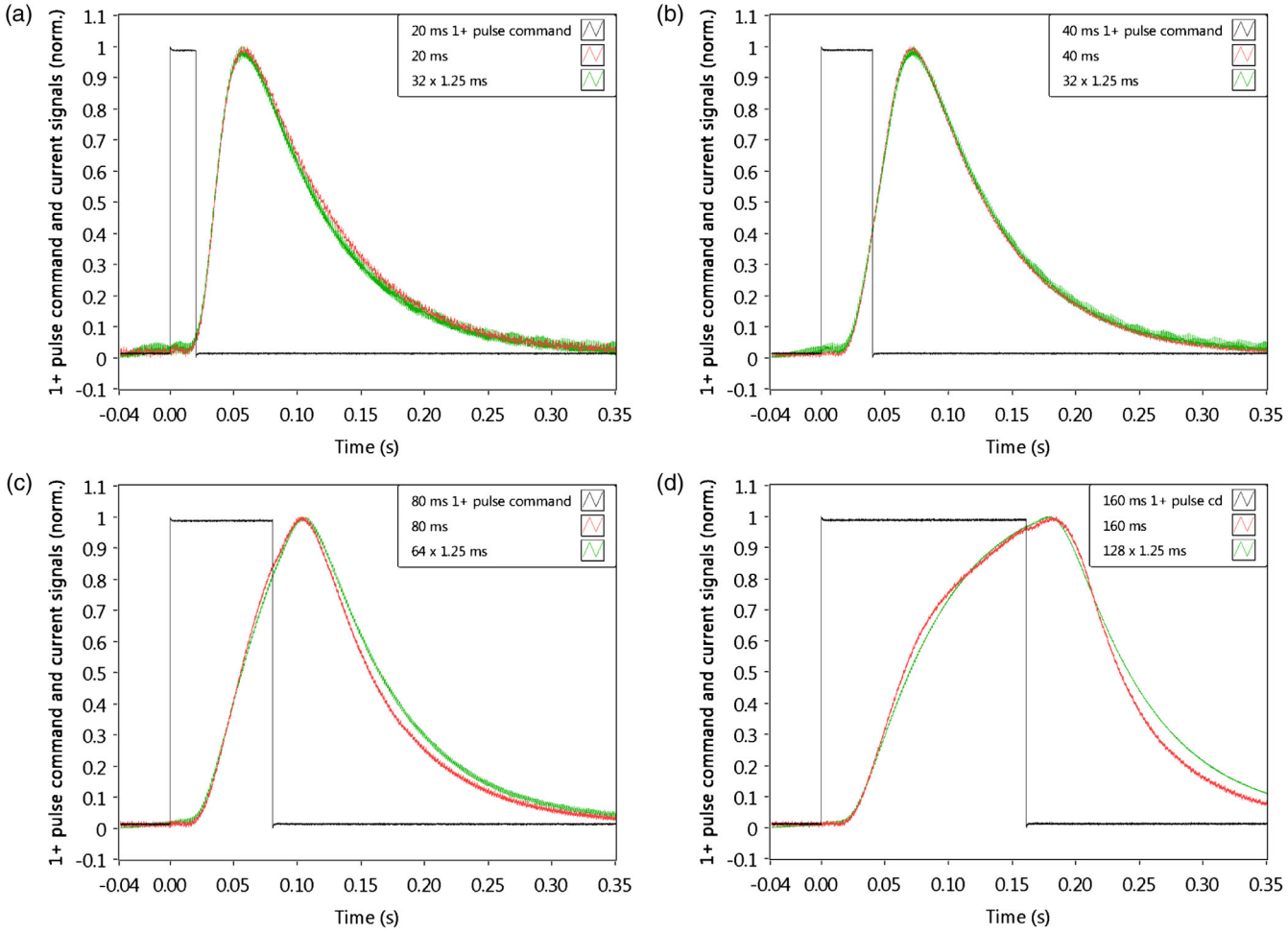

FIG. 9. N+ responses built from the duplication and sum of a 1.25 ms pulse response compared to measured N+ responses for 20 (a), 40 (b), 80 (c), and 160 ms (d) pulse durations. The curves are normalized in such a way that the maximum intensity is set to 1.

5. Accumulation effect

In order to test if the cumulative 1+ beam injection disturbs the CB plasma and has an influence on the charge breeding characteristic times, the long pulse response is compared to a signal $s(t)$ built from the temporal sum of short N+ pulse response arithmetically shifted by the 1+ pulse length δt, $s(t) = \sum_{i=1}^{P} I^{N+}(t - i\delta t)$ where $P\delta t$ is the long 1+ pulse length. Responses to long pulse durations of 20, 40, 60, and 120 ms (P = 16, 32, 64, and 128, respectively) are compared to curves built from individual $\delta t = 1.25$ ms pulse responses and plotted in Fig. 9.

The measured responses are well reproduced by the reconstructed curves. For 20 and 40 ms, the responses are identical while a slight accumulation effect appears beyond. It demonstrates, for this configuration, that the charge breeding process is mainly cumulative and that the general shape of the response curves are adding up quite linearly. The perturbation caused by the 1+ injection is not significantly changing the charge breeding timescales although it has been previously shown to affect the charge state distribution of the buffer gas plasma [20].

IV. FURTHER INVESTIGATIONS ON ACCUMULATION EFFECT

To go further, additional experiments were realized to compare the responses obtained at buffer gas equilibrium (perturbation by a short 1+ pulse injection) with the responses at the "final state," when the new equilibrium due to the accumulation of continuous injected ions in the plasma is reached. This investigation is motivated by the possibility of the buffer gas plasma equilibrium of the described short pulse experiments being different from the actual charge breeding equilibrium with continuous 1+ injection.

A. Method

In order to probe the final state plasma equilibrium, the 1+ beam is continuously injected into the charge breeder and the amplitude of the signal is modulated with a superimposed square pulse to induce a response of the N+ beam. Also in this case, the pulsing has to be done at low frequency, with a short duration. The amplitude of the superimposed pulse must be high enough to obtain a good signal-to-noise ratio but also low enough to cause a minimal perturbation of the charge breeder plasma. Figure 10 compares the principle of the two methods probing the two plasma states.

B. Experimental setup

In order to probe the N+ response at the final state equilibrium, the 1+ beam intensity had to be modulated promptly. To achieve that, the first electrode (puller) potential of the ion gun source [20] was modified. The puller electrode controls the ion extraction from the gun and allows a fast change of the beam intensity, changing slightly the beam emittance from 3.1 to 3.3 mm mrad (1σ, rms), which can be considered as a small change for the injection optics and capture process [24]. A fast high-voltage supply TREK 677B, set on the high voltage platform, was used to polarize the puller electrode with respect to the high voltage. It was driven by a signal generator and fast analog fiber optics (Analog modules 732 T/R-2.5-50). The rise and fall times of the voltage applied to the puller electrode of the ion gun were measured to be 180 μs for both the rise and fall times. The 1 + N+ test bench instrumentation was adapted to generate either the first or the second 1+ temporal signal of Fig. 10. This is essential to compare the responses under the same experimental conditions.

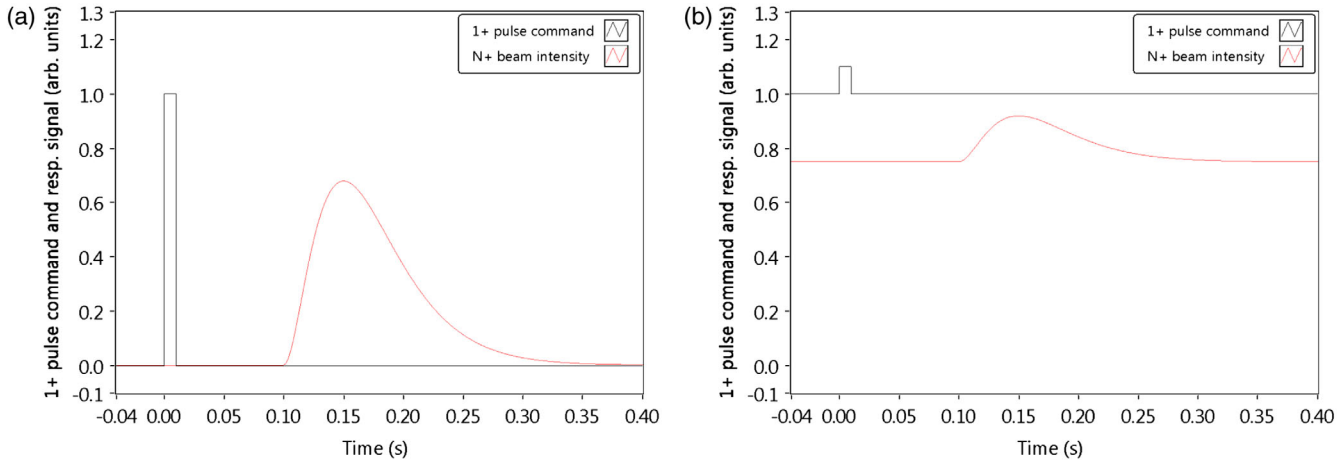

FIG. 10. Principle of the methods to probe the plasma at buffer gas equilibrium (a) and final state equilibrium (b).

C. Experimental results

To compare the temporal characteristics of the N+ responses in the two plasma states, $^{85}Rb^{+}$ pulses of 751 nA lasting 2.5 ms were first injected in the charge breeder. The injection, minimum, and extraction axial magnetic field strength were simulated to be 1.19, 0.44, and 0.83 T, respectively (injection, median, and extraction coils were set at 1180, 321, and 720 A). The microwave power level was 510 W and the buffer gas was He. An efficiency of 5% was measured for Rb^{19+} with the traditional method. A decrease of the puller electrode voltage from −200 to −240 V increased the 1+ beam intensity from 751 to 974 nA. While injecting the CW 1+ beam in the charge breeder with the puller set to −240 V, an efficiency of 4.6% was obtained without retuning the beam optics. This decrease of efficiency was probably due to a mismatch of the 1+ beam optics and it was considered negligible for this experiment.

For the charge states 4+, 8+, 13+, and 19+ of rubidium, the response signals were measured at buffer gas equilibrium (pulsing the 1+ current from 0 to 751 nA) and then at final state (pulsing the 1+ current from 751 to 974 nA), by switching from one to the other as fast as possible to ensure the same experimental conditions for both measurements.

The results are compared in Fig. 11 where the offset part of the signals is removed and a normalization factor is applied to obtain the same amplitude for the main pulse. Similar profiles were obtained for the curves of Rb^{4+}, Rb^{8+}, and Rb^{13+} in both initial equilibriums. For Rb^{19+} a prompt increase is noticed during the 1+ injection pulse followed by a dip before the main pulse response. The amplitudes of the fast pulse and the dip are higher when the 1+ injection is modulated instead of switching it completely on and off. A fast pulse has also been reported for the high charge state of Bismuth while injecting neutrals [17], the residual high charge state ions being presumably deconfined by the large burst of neutrals. In the case of 1 + ions injection, the fast pulse can be interpreted according to two causes that can combine. First, it would be due to the Coulomb collisions between the injected 1 + ions and the high charge state ions, the amount of N+ ions stored in the plasma being higher in the final state equilibrium. It can be hypothesized that the increase of the 1+ flux

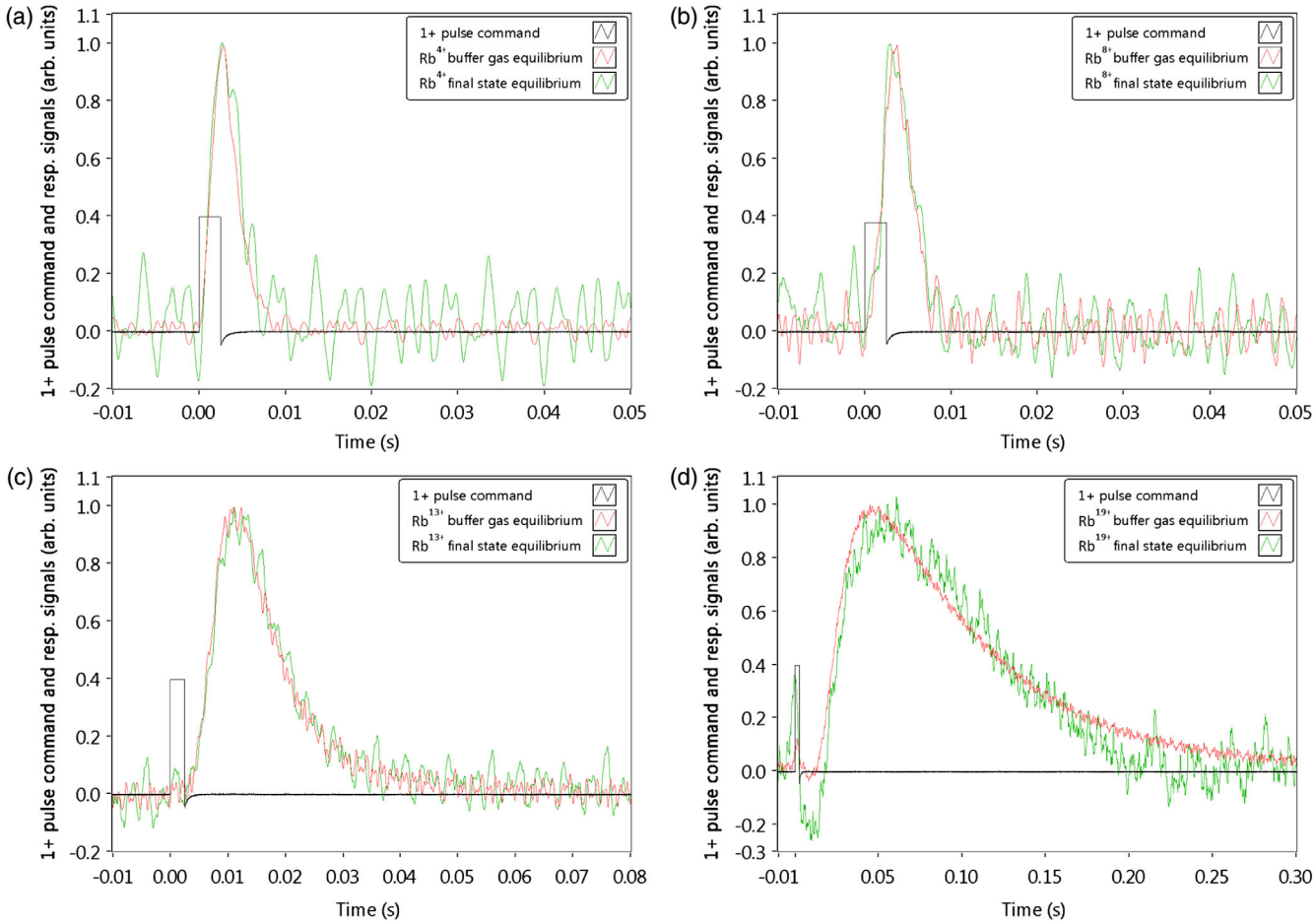

FIG. 11. Comparison of Rb^{4+} (a), Rb^{8+} (b), Rb^{13+}, (c) and Rb^{19+} (d) response signals in both plasma conditions.

TABLE IV. Estimation of the Rb^{19+} charge breeding efficiency of different Rb isotopes.

Isotope	^{85}Rb	^{93}Rb	^{94}Rb	^{95}Rb	^{96}Rb	^{97}Rb	^{98}Rb	^{99}Rb
$T_{1/2}$ (ms)	Stable	5840	2702	377.5	202.8	169.9	114	50.3
Rb^{19+} efficiency (%)	5.07	5.02	4.95	4.30	3.77	3.57	3.05	1.77
Rb^{19+}RIB efficiency/Rb^{19+}efficiency (%)	100	98.9	97.7	84.9	74.3	70.3	60.1	35

transfers energy to the high charge state ions and allows them to escape from the electrostatic potential dip [25] in the core plasma causing the peak of the Rb^{19+} current. The second assumption is that the potential dip would be modified (decreased) by the injected ions, changing the electric charge balance around the axis. The most sensitive species to potential dip being the high charge states, those would be more deconfined than lower ones. In both cases, the following drop of the current would be explained by a recovery from the transient first draining the ion reservoir.

In the case of Rb^{19+} the shape of the main pulse response is also slightly modified, the maximum being reached later in the case of final state equilibrium. This change of shape can be due to the first interaction which happened during the injection modulation and carried on through the main pulse. For Rb^{19+}, $\langle t \rangle$ is measured at 92.3 ms at buffer gas equilibrium, and 100.8 ms at final state equilibrium.

In this configuration, the two methods, i.e., injection at buffer gas equilibrium and final state equilibrium, give essentially the same results, but for high charge states, the response can be slightly affected by the beam injection.

V. IMPLICATIONS ON THE RIB CB EFFICIENCY

The N+ pulse response gives the temporal distribution of the ions extracted from the CB, the N+ responses being different depending on the charge state. During the CB development or the experiments preparing for RIB operation, stable ions are injected into the CB and the pulse efficiency can be calculated as shown above. In the case of a RIB, having a half-life $T_{1/2}$, the unstable isotopes population decay is of the form $N(t) = N_0 e^{\frac{-t}{\tau_1}}$ with $T_{1/2} = \tau_1 * \ln(2)$. Together with the pulse shapes recorded with stable isotopes this allows one to estimate the actual N+ RIB efficiency as a function of $T_{1/2}$. Accurate estimates require the 1+ pulse duration to be much shorter than $T_{1/2}$ (e.g., a factor of 10) as otherwise the start of the decay time is ambiguously defined. We emphasize here that such an estimate cannot be made based on the breeding time measured with the traditional long-pulse method, which highlights the value of the short pulse technique.

A. Efficiency as a function of the half-life

In the case of rubidium, a stable beam of $^{85}Rb^{+}$ could be used to preset the CB for the production of other radioactive Rb isotopes. With the 2.5 ms $^{85}Rb^{19+}$ pulse response of Fig. 6(a), the efficiencies of $^{93}Rb^{19+}$, $^{94}Rb^{19+}$, $^{95}Rb^{19+}$, $^{96}Rb^{19+}$, $^{97}Rb^{19+}$, $^{98}Rb^{19+}$, and $^{99}Rb^{19+}$ RIB are estimated and summarized in Table IV and Fig. 12. It is worse noting that, depending on the fine-tuning of the booster, the absolute efficiency for a given charge state can vary by $\pm 0.2\%$.

Figure 12 demonstrates that down to a half-life of about 380 ms, corresponding to $^{95}Rb^{19+}$, the reduction of efficiency is limited to about 15%, but at shorter half-lives the CB efficiency starts decreasing rapidly for this charge state.

B. Estimated RIB efficiency as a function of the charge state

The charge state dependence of the CB efficiency in the case of RIB can also be estimated. As shown in Table III, the pulsed injection mode efficiency exhibits a maximum at high charge state (17+) but on the other hand the CB process is faster for low charge state ions. This suggests that the optimum charge state for the stable beam efficiency is not always the best in the case of RIB. The N+ responses of the 4+, 8+, 10+, 13+, 17+, and 19+ charge state of ^{85}Rb of Fig. 6(a) are used to estimate the efficiencies of the corresponding charge states of radioactive Rb isotopes. The charge state distributions are shown in Fig. 13(a) and the evolution of the average charge state as a function of the half-life in Fig. 13(b). For short-lived isotopes such as ^{99}Rb, the charge state distribution is shifted toward lower

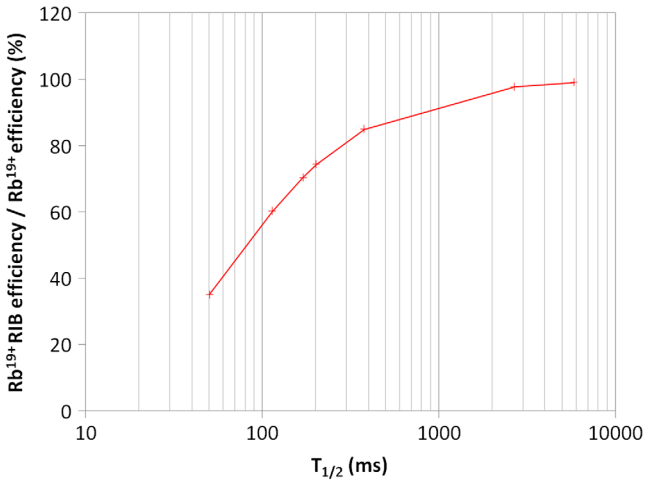

FIG. 12. Evolution of the Rb^{19+} RIB efficiency over Rb^{19+} stable efficiency ratio as a function of $T_{1/2}$.

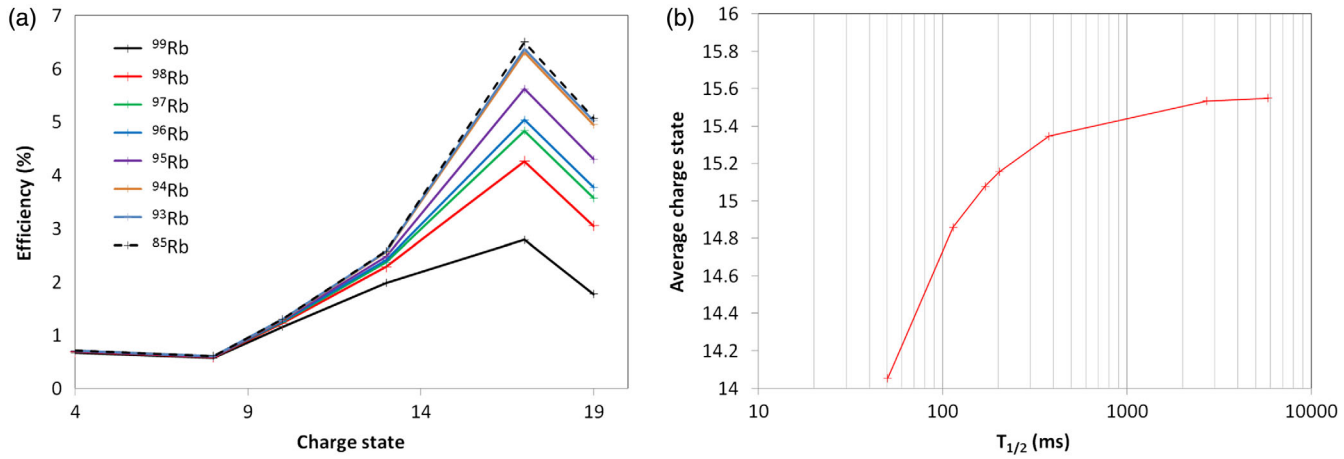

FIG. 13. (a) Rb isotope efficiencies as a function of the charge state. (b) Evolution of the average charge state as a function of the half-life.

charge states due to decay losses. In this case, a decrease of about 1.6 is noticed for ^{99}Rb with respect to ^{85}Rb.

VI. CONCLUSION

In this study, investigations on the charge breeding time have been performed using short 1+ pulse injection as a new tool to provide information on the temporal distribution of the multicharged ions extracted from an ECRIS charge breeder. For Rb^{19+}, the efficiency in the short pulse mode is found comparable to the traditional measurement technique.

The short pulse method proposed in this work has demonstrated that the accumulation effect (i.e., self-consistent perturbation of the plasma equilibrium induced by injected ion accumulation) is negligible in the studied configuration (i.e., injected 1+ beam intensity from 177 to 644 nA and 1+ pulse duration from 1 to 120 ms). The 90% charge breeding times measured with the traditional method were found to be slightly longer (by 9%) than those obtained in short pulse mode.

The short pulse method provides extra information on the time characteristics of the N+ responses, and allows us to study the CB plasma behavior as a function of the charge breeder tuning parameters. In the future, the response curves will be systematically recorded during the charge breeder qualification experiments. This will allow one to compare different configurations of the charge breeder that are planned within the development program that includes important modifications of the magnetic structure.

During the 1+ beam injection, a prompt interaction is noticed between the injected ions and the high charge state ones trapped in the plasma causing their deconfinement. This indicates that the 1+ beam injection disturbs the plasma equilibrium close to the axis. Possible explanations are (i) an energy transfer between the injected ions and the high charge state ones allowing them to pass the potential dip, (ii) a modification of the potential dip due to the charges delivered by the injected ions, or (iii) a combination of these two assumptions.

Finally, the N+ response curves enable more accurate measurements and estimates of the charge breeding times and efficiencies of radioactive isotopes than measurements with the traditional technique. They allow one to estimate more precisely the global efficiency of the ISOL chain as a function of the radioactive ion beam half-life and charge state. With this technique, a database summarizing all the estimated RIB efficiencies and response curves of different elements, isotopes, and charge states can be built for the ISOL community using ECR charge breeders.

[1] M. Lindroos, Review of ISOL-type radioactive beam facilities, in *Proceedings of EPAC2004, Lucerne, Switzerland* (JACoW, CERN, Geneva, Switzerland, 2004), TUXCH01.

[2] L. Maunoury, P. Delahaye, M. Dubois, O. Bajeat, C. Barthe-Dejean, R. Frigot, P. Jardin, A. Jeanne, O. Kamalou, P. Lecomte, B. Osmond, G. Peschard, A. Savalle, J. Angot, T. Lamy, and P. Sole, SPIRAL1 charge breeder: Performances and status, in *Proceedings of ECRIS2016, Busan, South Korea* (JACoW, CERN, Geneva, Switzerland, 2016), MOFO01.

[3] R. Vondrasek, J. Clark, A. Levand, T. Palchan, R. Pardo, G. Savard, and R. Scott, Operational experience with the Argonne National Laboratory Californium Rare Ion Breeder Upgrade facility and electron cyclotron resonance charge breeder, Rev. Sci. Instrum. **85**, 02B903 (2014).

[4] R. Geller, T. Lamy, and P. Sortais, Charge breeding of isotope on-line-created radioactive ions using an electron cyclotron resonance ion trap, Rev. Sci. Instrum. **77**, 03B107 (2006).

[5] S. C. Jeong, M. Oyaizu, E. Tojyo, H. Kawakami, H. Ishiyama, H. Miyatake, K. Enomoto, Y. Watanabe, I. Katayama, T. Nomura, M. Matsuda, A. Osa, and S. Ichikawa, Test results of 18 GHz ECR charge breeder

for KEK–JAERI RNB facility, Rev. Sci. Instrum. **75**, 1631 (2004).

[6] F. Ames, R. Baartman, P. Bricault, K. Jayamanna, M. McDonald, M. Olivo, P. Schmor, D. H. L. Yuan, and T. Lamy, Charge state breeding of radioactive ions with an electron cyclotron resonance ion source at TRIUMF, Rev. Sci. Instrum. **77**, 03B103 (2006).

[7] L. Maunoury, P. Delahaye, M. Dubois, J. Angot, P. Sole, O. Bajeat, C. Barton, R. Frigot, A. Jeanne, P. Jardin, O. Kamalou, P. Lecomte, B. Osmond, G. Peschard, T. Lamy, and A. Savalle, Charge breeder for the SPIRAL1 upgrade: Preliminary results, Rev. Sci. Instrum. **87**, 02B508 (2016).

[8] T. Lamy, J. L. Bouly, J. C. Curdy, R. Geller, A. Lacoste, P. Sole, P. Sortais, T. Thuillier, J. L. Vieux-Rochaz, K. Jayamanna, M. Olivo, P. Schmor, and D. Yuan, Charge state breeding applications with the ECR PHOENIX source: From low to high current production, Rev. Sci. Instrum. **73**, 717 (2002).

[9] O. Tarvainen, T. Lamy, J. Angot, T. Thuillier, P. Delahaye, L. Maunoury, J. Choinski, L. Standylo, A. Galata, G. Patti, and H. Koivisto, Injected $1+$ ion beam as a diagnostics tool of charge breeder ECR ion source plasmas, Plasma Sources Sci. Technol. **24**, 035014 (2015).

[10] O. Tarvainen, J. Angot, I. Izotov, V. Skalyga, H. Koivisto, T. Thuillier, T. Kalvas, and T. Lamy, Plasma instabilities of a charge breeder ECRIS, Plasma Sources Sci. Technol. **26**, 105002 (2017).

[11] R. Vondrasek, P. Delahaye, S. Kutsaev, and L. Maunoury, Improved charge breeding efficiency of light ions with an electron cyclotron ion source, Rev. Sci. Instrum. **83**, 113303 (2012).

[12] J. Angot, T. Thuillier, O. Tarvainen, M. Baylac, J. Jacob, T. Lamy, M. Migliore, and P. Sole, Recent improvements of the LPSC Charge Breeder, in *Proceedings of ICIS2017, Geneva, Switzerland, T6_Tu_65* (to be published).

[13] O. Tarvainen, J. Angot, I. Izotov, V. Skalyga, H. Koivisto, T. Thuillier, T. Kalvas, V. Toivanen, R. Kronholm, and T. Lamy, The effect of plasma instabilities on the background impurities in charge breeder ECRIS, in *Proceedings of ICIS2017, Geneva, Switzerland, T6_Tu_66* (to be published).

[14] V. Mironov, S. Runkel, K. E. Stiebing, O. Hohn, G. Shirkov, H. Schmidt-Böcking, and A. Schempp, Plasma diagnostics at electron cyclotron resonance ion sources by injection of laser ablated fluxes of metal atoms, Rev. Sci. Instrum. **72**, 2271 (2001).

[15] T. Nakagawa, T. Aihara, Y. Higurashi, M. Kidera, M. Kase, Y. Yano, I. Arai, H. Arai, M. Imanaka, S. M. Lee, G. Arzumanyan, and G. Shirkov, Electron cyclotron resonance ion source developments in RIKEN (invited), Rev. Sci. Instrum. **75**, 1394 (2004).

[16] R. C. Vondrasek, R. H. Scott, R. C. Pardo, and D. Edgell, Techniques for the measurement of ionization times in ECR ion sources using a fast sputter sample and fast gas valve, Rev. Sci. Instrum. **73**, 548 (2002).

[17] R. C. Pardo, R. Harkewicz, and P. J. Billquist, Time evolution of charge states in an electron cyclotron resonance ion source, Rev. Sci. Instrum. **67**, 1602 (1996).

[18] N. Chauvin, J. F. Bruandet, J. L. Bouly, J. C. Curdy, R. Geller, T. Lamy, P. Sole, P. Sortais, and J. L. Vieux-Rochaz, The $1^+ \rightarrow n^+$ charge breeding method for the production of radioactive and stable continuous/pulsed multi-charged ion beams, in *Proceedings of the International Workshop on ECR Sources, Geneva, Switzerland, 1999*, edited by B. Allardyce, H. Haseroth, C. Hill, and K. Langbein, pp. 151–154, https://cds.cern.ch/record/396666?ln=en.

[19] P. Sortais, T. Lamy, J. Médard, J. Angot, L. Latrasse, and T. Thuillier, Ultracompact/ultralow power electron cyclotron resonance ion source for multipurpose applications, Rev. Sci. Instrum. **81**, 02B314 (2010).

[20] T. Lamy, J. Angot, T. Thuillier, P. Delahaye, L. Maunoury, J. Choinski, L. Standylo, A. Galata, G. Patti, H. Koivisto, and O. Tarvainen, Experimental activities with the LPSC charge breeder in the European context, in *Proceedings of ECRIS 2014, Nizhny Novgorod, Russia* (JACoW, CERN, Geneva, Switzerland, 2014), WEOBMH01.

[21] T. Lamy, J. Angot, M. Marie-Jeanne, J. Medard, P. Sortais, T. Thuillier, A. Galata, and H. Koivisto, Fine frequency tuning of the PHOENIX charge breeder used as a probe for ECRIS plasmas, in *Proceedings of ECRIS 2010, Grenoble, France* (JACoW, CERN, Geneva, Switzerland, 2010), WEKOBK03.

[22] H. I. West Jr., Calculation of ion charge-state distribution in ECR ion sources, Lawrence Livermore National Laboratory Report No. UCRL-53391, 1982.

[23] D. Neben, G. Machicoane, G. Parsey, A. Pham, J. Stetson, and J. Verboncoeur, An analysis of fast sputtering studies for ion confinement time, in *Proceedings of LINAC2016, East Lansing, USA* (JACoW, CERN, Geneva, Switzerland, 2016), TUPCR032.

[24] A. Galatà, D. Mascali, G. Torrisi, L. Neri, L. Celona, and J. Angot, Influence of the injected beam parameters on the capture efficiency of an electron cyclotron resonance based charge breeder, Phys. Rev. Accel. Beams **20**, 063401 (2017).

[25] G. Shirkov, Multiconponent consideration of electron fraction of electron-cyclotron resonance source plasma, Rev. Sci. Instrum. **71**, 850 (2000).